PYROEFFECTS ON MULTIPHASE MAGNETO-ELECTRO-ELASTIC SENSOR PATCH BONDED ON MILD STEEL PLATE

P Kondaiah[1]*, K Shankar[2], and N Ganesan[3]

[1]Mahindra Ecole Centrale college of Engineering, Hyderabad, India 500043

[2,3]Machine Design Section, Dept. of Mechanical Engineering, IIT Madras, Chennai, India 600036

Emails: kondaiah.iitm@gmail.com, skris@iitm.ac.in, nganesan@iitm.ac.in

Submitted: Apr. 15, 2014 ***Accepted: June 27, 2014*** ***Published: Sep. 1, 2014***

Abstract- The magneto-electro-elastic (MEE) material under thermal environment exhibits pyroelectric and pyromagnetic coefficients resulting in pyroeffects such as pyroelectric and pyromagnetic. The pyroelectric and pyromagnetic effects on the behavior of multiphase MEE sensors bonded on the top surface of a mild steel plate under thermal environment is presented in this paper. The aim of the study is to investigate how samples having different volume fractions of the multiphase MEE sensor behave due to pyroeffects using finite element method. This is studied at an optimal location on the plate, where the maximum electric and magnetic potentials of the MEE sensor are induced due to pyroeffects under various boundary conditions. It is assumed that plate and sensor are perfectly bonded to each other. The maximum pyroelectric and pyromagnetic effects on electric and magnetic potentials are observed when volume fraction is v_f = 0.2. Additionally, the boundary conditions significantly influence the pyroelectric and pyromagnetic effects on electric and magnetic potentials of the sensor.

Index terms*:* magneto-electro-elastic sensor, pyroelectric, pyromagnetic, finite element.

I. INTRODUCTION

Magneto-Electro-Elastic (MEE) materials belong to the family of smart materials; they have the ability to generate magnetic, electric and mechanical responses when subjected to a thermal stimulus due to their significant coupling between mechanical, electric, magnetic and thermal fields. MEE material exhibits magnetic-electric-mechanical coupling effect in such a way that they produce electric and magnetic fields when deformed and conversely, undergo deformation when subjected to electric and magnetic field. The magnetoelectric coupling effect which is absent in the constituent components is exhibited by this class of material. In addition to this, the pyroelectric and pyromagnetic coupling effects which are present with a thermal field are also exhibited by this class of MEE materials. This cross or product property is created by coupling of elastic deformations in the piezoelectric and piezomagnetic phases and the elastic deformations may be induced directly by mechanical loading/temperature gradient or indirectly by an application of electric or magnetic field. This unique feature allows magnetic control of electric polarization, electric control of magnetization and control of electric and magnetic fields with mechanical stress. Due to exceptional nature of these materials to convert one form of energy into another, find widespread applications in areas like magnetic field probes, acoustic devices, medical ultrasonic imaging, sensors and actuators Wu and Huang [1].

Aboudi [2] has presented the effective moduli of magneto-electro-elastic composite by employing homogenization method with the assumption that composites have a periodic structure. Sunar *et al*. [3] has presented finite element modeling of a fully coupled thermopiezomagnetic continuum with the aid of thermodynamic potential. Sirohi *et al.* [4] investigated the piezoceramic (PZT) strain sensors by measuring the strain generated by direct piezoelectric effect. Mahieddine and Ouali [5] have used finite element model is to analyze beams with piezoelectric sensors and actuators based on first order Kirchoff theory. Various parametric studies were conducted to demonstrate the application of piezoelectric effect in active vibration control. Daga *et al.* [6] has presented the transient sensory response of magneto-electro-elastic composite containing different volume fractions of Barium Titanate ($BaTiO_3$) in a matrix of Cobalt Iron Oxide ($CoFe_2O_4$) by using magnetic scalar potential approach.

Soh and Liu [7] have presented the recent research advances on the magnetoelectric coupling effect of piezoelectric-piezomagnetic composite materials and their fundamental mechanics

issues are reviewed comprehensively. The eight sets of constitutive equations for magnetoelectroelastic solids and the energy functions corresponding to each set of constitutive equations are given. The mathematical properties of the thermodynamic potentials and the relations between the material constants are discussed. Ryu *et al.*[8]have investigated ME particulate composites and laminate composites and summarized the important results. After a review of data in the literature, they concluded that in order to obtain excellent ME property from the ME laminate composites, a high piezoelectric voltage coefficient, an optimum thickness ratio between piezoelectric layer and Terfenol-D layers, the direction of magnetostriction in the Terfenol-D disks, and higher elastic compliance of piezoelectric material were important factors. Nan *et al.* [9] studied bulk and nanostructured multiferroic MEE composite consisting of ferroelectric and magnetic phases in experimental and theoretical perspectives. The effects of geometric size and mechanical boundary conditions on bilayered composites for magneto-electric coupling was investigated by Pan *et al.* [10] using three dimensional finite element approach. The theoretical analysis of a multilayered magneto-electro-thermoelastic hallow cylinder under unsteady and uniform surface heating is presented by Ootao and Ishihara [11]. The exact solution of transient thermal stress problem with the assumption of plane strain state is obtained. Additionally without considering the pyroelectric and pyromagnetic effects they investigated the effects of coupling between magnetic, electric and thermoelastic fields. Guiffard *et al.*[12] were studied room temperature magnetic field detection using a single piezoelectric disk with good sensitivity and linear response versus DC magnetic field change. This study validates that ME effect originates from the presence of eddy currents within the metal electrodes of the ceramic.

Recently, Hadjiloizi *et al.* [13] have presented the effective pyroelectric and pyromagnetic coefficients in micromechanical analysis of magneto-electro-thermo-elastic composite for quasi-static model using the asymptotic homogenization method. The results of this model fully agree with Bravo-Castillero *et al.* [14].Study of these pyroelectric and pyromagnetic coefficients resulting in pyroelectric and pyromagnetic effects on MEE sensor to account the thermal environment for enhancing the performance of the sensor was uncovered till date. Hence the present work is attempted.

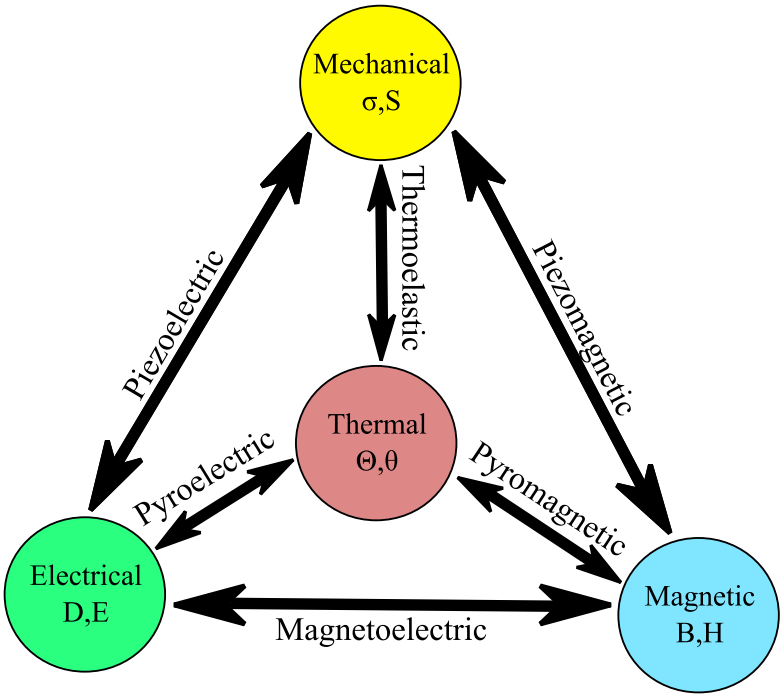

Fig.1 Schematic diagram showing the complex mechanical, electric, magnetic and thermal coupling [19].

II. THEORETICAL FORMULATION

A. Constitutive Equations

Multiphase magneto-electro-elastic (MEE) material having piezoelectric phase and piezomagnetic phase under thermal environment exhibits the coupling between mechanical, electrical, magnetic and thermal fields as shown in Fig. 1.The constitutive equations for multiphase magneto-electro-elastic three dimensional solid under thermal environment (temperature field not fully coupled with the magneto-electro-elastic field) in a rectangular Cartesian coordinate system (x,y,z) are shown in (1). These equations relating stress σ_j, electric displacement D_l, and magnetic flux density B_l to strain S_k, electric field E_m, magnetic field H_m and thermal field Θ. Linear coupling is assumed between magnetic, electric, thermal and elastic fields (Sunar *et al.* [3]; Gao and Noda [15]).

$$\left.\begin{aligned}\sigma_j &= c_{jk}S_k - e_{mj}E_m - q_{mj}H_m - \gamma_j\Theta \\ D_l &= e_{lk}S_k + \varepsilon_{lm}E_m + m_{lm}H_m + p_l\Theta \\ B_l &= q_{lk}S_k + m_{lm}E_m + \mu_{lm}H_m + \tau_l\Theta\end{aligned}\right\} \quad (1)$$

wherec_{jk}, e_{lk}, q_{lk}, are elastic, piezoelectric and piezomagnetic coefficients respectively and γ_j is the thermal stress coefficient being related with the thermal expansion coefficient β by $\gamma = c\beta$. ε_{lm}, m_{lm}, μ_{lm}, λ_{lk}, p_l, and τ_l represents respectively the dielectric, magneto-electric, magnetic permeability, thermal conductivity, pyroelectric and pyromagnetic coefficients. Here j, k = 1,...,6 and l, m = 1,...,3. The standard contraction of indices has been used for the elastic constants (i.e. $S_4 = S_{24}$ etc.).

B. Finite Element Modeling

For finite element formulation of a coupled system, the displacements $\{u\}=\{u_x, u_y, u_z\}^T$, electrical potential $\{\phi\}$ and magnetic potential $\{\psi\}$ within element in terms of suitable shape functions can be written as,

$$\begin{aligned}u^e &= \left[N_u\right]\{u_i\} \\ \phi^e &= \left[N_\phi\right]\{\phi_i\} \\ \psi^e &= \left[N_\psi\right]\{\psi_i\}\end{aligned} \quad (2)$$

where the subscripts e and i respectively stand for the element and nodes of the element and N are the shape function matrices whose subscripts denote the associated fields.

The derivation of finite element equations for magneto-electro-thermo-elastic solid by using virtual displacement principle is given by Ganesan *et al.* [16] and is written in the coupled form as,

$$\begin{bmatrix} M^e_{uu} & 0 & 0 & 0 \\ 0 & 0 & 0 & 0 \\ 0 & 0 & 0 & 0 \\ 0 & 0 & 0 & 0 \end{bmatrix}\begin{Bmatrix}\ddot{u}^e \\ \ddot{\phi}^e \\ \ddot{\psi}^e \\ \ddot{\Theta}^e\end{Bmatrix} + \begin{bmatrix} 0 & 0 & 0 & -C^e_{u\Theta} \\ 0 & 0 & 0 & 0 \\ 0 & 0 & 0 & 0 \\ C^e_{\Theta u} & -C^e_{\Theta\phi} & -C^e_{\Theta\psi} & C^e_{\Theta\Theta} \end{bmatrix}\begin{Bmatrix}\dot{u}^e \\ \dot{\phi}^e \\ \dot{\psi}^e \\ \dot{\Theta}^e\end{Bmatrix}$$
$$+ \begin{bmatrix} K^e_{uu} & K^e_{u\phi} & K^e_{u\psi} & -K^e_{u\Theta} \\ K^e_{\phi u} & -K^e_{\phi\phi} & -K^e_{\phi\psi} & K^e_{\phi\Theta} \\ K^e_{\psi u} & -K^e_{\psi\phi} & -K^e_{\psi\psi} & K^e_{\psi\Theta} \\ 0 & 0 & 0 & K^e_{\Theta\Theta} \end{bmatrix}\begin{Bmatrix}u^e \\ \phi^e \\ \psi^e \\ \Theta^e\end{Bmatrix} = \begin{Bmatrix} f^e_u + T^e_u \\ 0 \\ 0 \\ -T^e_\Theta \end{Bmatrix} \quad (3)$$

The dynamic behavior of the coupled magneto-electro-thermo-elastic structure is investigated using (3). The prominent contribution of the present work is to formulate the pyroelectric and

pyromagnetic effects for three dimensional magneto-electro-elastic structures under thermal environment using finite element method. To investigate the pyroelectric and pyromagnetic effects, the damping condition is not considered in (3), and is reduced to static case along with the following assumptions,

1. Thermal field of the system is uniform and not fully coupled with the magneto-electro-elastic field, *i.e.*, the magneto-electro-elastic field can be affected by the temperature field through constitutive relations, but the temperature field is not affected by the magneto-electro-elastic field.
2. The mechanical, electric and magnetic fields are fully coupled.
3. The externally applied mechanical force, electric charge and magnetic current are assumed to be zero.

Based on the above assumptions, (3) can be written without considering body and traction forces as,

$$\left.\begin{aligned}
\left[K^e{}_{uu}\right]\left\{u^e\right\}+\left[K^e{}_{u\phi}\right]\left\{\phi^e\right\}+\left[K^e{}_{u\psi}\right]\left\{\psi^e\right\}&=\left\{0+F^e_{u\Theta}\right\}\\
\left[K^e{}_{u\phi}\right]^T\left\{u^e\right\}-\left[K^e{}_{\phi\phi}\right]\left\{\phi^e\right\}-\left[K^e{}_{\phi\psi}\right]\left\{\psi^e\right\}&=\left\{0-F^e_{\phi\Theta}\right\}\\
\left[K^e{}_{u\psi}\right]^T\left\{u^e\right\}-\left[K^e{}_{\phi\psi}\right]^T\left\{\phi^e\right\}-\left[K^e{}_{\psi\psi}\right]\left\{\psi^e\right\}&=\left\{0-F^e_{\psi\Theta}\right\}
\end{aligned}\right\} \qquad (4)$$

where $\{F^e_{u\Theta}\}$, $\{F^e_{\phi\Theta}\}$ and $\{F^e_{\psi\Theta}\}$ represents the thermal, pyroelectric and pyromagnetic load vectors respectively, and these are explained in Section *C.* (Note: The negative signs of $\{F^e_{\phi\Theta}\}$ and $\{F^e_{\psi\Theta}\}$ in (4) are taken care of by pyroelectric and pyromagnetic properties in Table1). The matrix $K^e_{u\phi}$ is element stiffness matrix due to piezoelectric-mechanical coupling effect, and $K^e_{u\psi}$ is element stiffness matrix due to piezomagnetic-mechanical coupling effect, and $K^e_{\phi\psi}$ is element stiffness matrix due to magneto-electric coupling effect. $K^e_{u\Theta}$, $K^e_{\phi\Theta}$ and $K^e_{\psi\Theta}$ are element stiffness matrices due to thermal-mechanical, thermal-electrical and thermal-magnetic coupling effects respectively. The matrices K^e_{uu}, $K^e_{\phi\phi}$ and $K^e_{\psi\psi}$ are element stiffness matrices due to mechanical, electrical and magnetic fields respectively.

C. Evaluation of Elemental Matrices

The different elemental matrices of (4) for magneto-electro-elastic solid are further defined as,

$$\left[K^e_{uu}\right]=\int_v\left[B_u\right]^T[c]\left[B_u\right]dv;\ \left[K^e_{u\phi}\right]=\int_v\left[B_u\right]^T[e]\left[B_\phi\right]dv;$$
$$\left[K^e_{u\psi}\right]=\int_v\left[B_u\right]^T[q]\left[B_\psi\right]dv;\ \left[K^e_{\phi\psi}\right]=\int_v\left[B_\phi\right]^T[m]\left[B_\psi\right]dv;$$
$$\left[K^e_{\phi\phi}\right]=\int_v\left[B_\phi\right]^T[\varepsilon]\left[B_\phi\right]dv;\ \left[K^e_{\psi\psi}\right]=\int_v\left[B_\psi\right]^T[\mu]\left[B_\psi\right]dv$$

In the present study, for a specified uniform temperature rise (Θ), the thermal load, equivalent pyroelectric load (electric load generated due to temperature) and pyromagnetic load (magnetic load generated due to temperature) terms are calculated, and applied as external loads in the system equations given in (4). These can be solved for displacements, electric potential and magnetic potential. These external vectors used in the system equations are given as follows,

$$\left\{F^e_{u\Theta}\right\}=\left[K^e_{u\theta}\right]\left\{\Theta\right\}=\int_v\left[B_u\right]^T[c][\beta]\Theta dxdydz \tag{5}$$

where $\{F^e_{u\Theta}\}$ is the thermal load vector and is governed as a direct effect on displacements, and indirect effect on electric and magnetic potentials through constitutive equations.

$$\left\{F^e_{\phi\Theta}\right\}=\left[K^e_{\phi\Theta}\right]\left\{\Theta\right\}=\int_v\left[B_\phi\right]^T[p]\Theta dxdydz \tag{6}$$

where $\{F^e_{\phi\Theta}\}$ is the pyroelectric load vector and is governed as a direct effect on electric potential, and indirect effect on magnetic potential and displacement through constitutive equations.

$$\left\{F^e_{\psi\Theta}\right\}=\left[K^e_{\psi\Theta}\right]\left\{\Theta\right\}=\int_v\left[B_\psi\right]^T[\tau]\Theta dxdydz \tag{7}$$

where $\{F^e_{\psi\Theta}\}$ is the pyromagnetic load vector and it is governed as a direct effect on magnetic potential, and indirect effect on electric potential and displacements through constitutive equations.

The coupled formation of (4) can be written as

$$\begin{bmatrix}K_{uu} & K_{u\phi} & K_{u\psi}\\ K_{\phi u} & -K_{\phi\phi} & -K_{\phi\psi}\\ K_{\psi u} & -K_{\psi\phi} & -K_{\psi\psi}\end{bmatrix}\begin{Bmatrix}u\\ \phi\\ \psi\end{Bmatrix}=\begin{Bmatrix}F_{u\Theta}\\ F_{\phi\Theta}\\ F_{\psi\Theta}\end{Bmatrix} \tag{8}$$

III. RESULTS AND DISCUSSION

The finite element method is used to analyze the pyroeffects on the behavior of a magneto-electro-elastic sensor bonded to a mild steel plate subjected to uniform temperature rise of 50 K.

The purpose of the sensor is to measure electric and magnetic response to aapplied thermal environment. The main objective of the present work is to find out how samples having different volume fractions of the multiphase MEE sensor behave due to pyroeffects.The sensor bonded on top surface of the plate at optimal location (at the middle of the clamped edge) is considered based on optimal sensor placement study as discussed in Section III - *B*. The advantage of considering optimal sensor placement study is that there is no need to analyze the sensor behavior at selective locations such as clamped end, intermediate location, free end, etc.The multiphase MEE sensor is made of piezomagnetic ($CoFe_2O_4$) matrix reinforced by piezoelectric ($BaTiO_3$) material for different volume fractions $v_f = 0.0$ to $v_f = 1.0$ in steps of 0.2. The $v_f = 1.0$ corresponds to pure piezoelectric material and $v_f = 0.0$ corresponds to pure piezomagnetic material.

The pyroelectric effect can manifest in MEE sensor through the pyroelectric load (*Refer* (6)) when the plate is subjected to uniform temperature rise. Similarly, the pyromagnetic effect can manifest through the pyromagnetic load (*Refer* (7)). Influence of both the pyrolectric and pyromagnetic loads are referred to as direct effect on electric and magnetic potentials respectively. Indirectly, the values of electric and magnetic potentials due to thermal load (*Refer* (5)) can be developed through constitutive equations (*Refer* (1)). This is called indirect effect on electric and magnetic potentials (*Refer* Section II - *C*). Whereas in the case of displacement, it is vice-versa.

The plate is modeled with 8 node isoparametric element with sufficient number of elements across the thickness direction to capture the bending behavior of the plate correctly. The dimensions of the 3D plate and the sensor used for analysis are 0.3×0.3×0.006 m and 0.06×0.06×0.003 m respectively. The plate is subjected to CCCC, CFFC and FCFC boundary conditions (where 'C' stands for clamped *i.e.* $\{u, \phi, \psi\} = 0$ and 'F' for free *i.e.* $\{u, \phi, \psi\} \neq 0$ boundary condition) so as to investigate the influence of boundary condition for comparative studies. The three boundary conditions chosen are one symmetric boundary condition (CCCC), two adjacent free edges (CFFC) and two opposite free edges (FCFC). Fig.2 shows the finite element discretization of the mild steel plate with sensor bonded at the middle of the clamped edge.The material properties are given in Table 1. An optimum mesh size is chosen which give results within acceptable limits. The arrangement consists of one electrode from the plate which is grounded and the other electrode which is kept on the top of the sensor patch. The magnetic potentials are assumed to be zero at the clamped end.

To study the pyroelectric and pyromagnetic effects on bonded MEE sensor, the results are compared with conventional approach which presumed as without considering pyroelectric and pyromagnetic loads orin other words, the coefficients $\gamma \neq 0$, $p = 0$ and $\tau = 0$.

Table 1.Material properties of PZT5A and different volume fraction of multiphase magneto-electro-elastic $BaTiO_3$-$CoFe_2O_4$ [2], [13], [17], [18].

	$0.0v_f$	$0.2v_f$	$0.4v_f$	$0.6v_f$	$0.8v_f$	$1.0v_f$	PZT-5A
Elastic constants							
$C_{11}=C_{22}$	286	250	225	200	175	166	99.2
C_{12}	173	146	125	110	100	77	54
$C_{13}=C_{23}$	170	145	125	110	100	78	50.8
C_{33}	269.5	240	220	190	170	162	86.9
$C_{44}=C_{55}$	45.3	45	45	45	50	43	21.1
Piezoelectric constants							
$e_{31}=e_{32}$	0	-2.0	-3.0	-3.5	-4.0	-4.4	-7.2
e_{33}	0	4.0	7.0	11.0	14.0	18.6	15.1
$e_{24}=e_{15}$	0	0	0	0	0	11.6	12.3
Dielectric constants							
$\varepsilon_{11}= \varepsilon_{22}$	0.08	0.33	0.8	0.9	1.0	11.2	1.53
ε_{33}	0.093	2.5	5.0	7.5	10.0	12.6	1.5
Magnetic permeability constants							
$\mu_{11}= \mu_{22}$	-5.9	-3.9	-2.5	-1.5	-0.8	0.05	0
μ_{33}	1.57	1.33	1.0	0.75	0.5	0.1	0
Piezomagnetic constant							
$q_{31}=q_{32}$	580	410	300	200	100	0	0
q_{33}	700	550	380	260	120	0	0
$q_{24}=q_{15}$	560	340	220	180	80	0	0
Magnetoelectric constants							
$m_{11}=m_{22}$	0	2.8	4.8	6.0	6.8	0	0
m_{33}	0	2000	2750	2500	1500	0	0
Pyroelectric constants							
p_2	0	-3.5	-6.5	-9	-10.8	0	
Pyromagnetic constants							
τ_2	0	-36	-28	-18	-8.5	0	0
Thermal expansion coefficient							
$\beta_{11}= \beta_{22}$	10	10.8	11.8	12.9	14.1	15.7	1.5
β_{33}	10	9.3	8.6	7.8	7.2	6.4	1.5
Density							
P	5300	5400	5500	5600	5700	5800	7750

c_{ij} in N/m^2, e_{ij} in C/m^2, ε_{ij}in 10^{-9} $C^2/N\ m^2$ or $10^{-9}C/V\ m$,q_{ij} in N/A m, μ_{ij} in $10^{-4}Ns^2/C^2$, m_{ij} in 10^{-12} N s/V C,p_i in 10^{-7} $C/m^2\ K$, τ_i in 10^{-5} $C/m^2\ K$, β_{ij} in 10^{-6} 1/K, ρ in kg/m^3

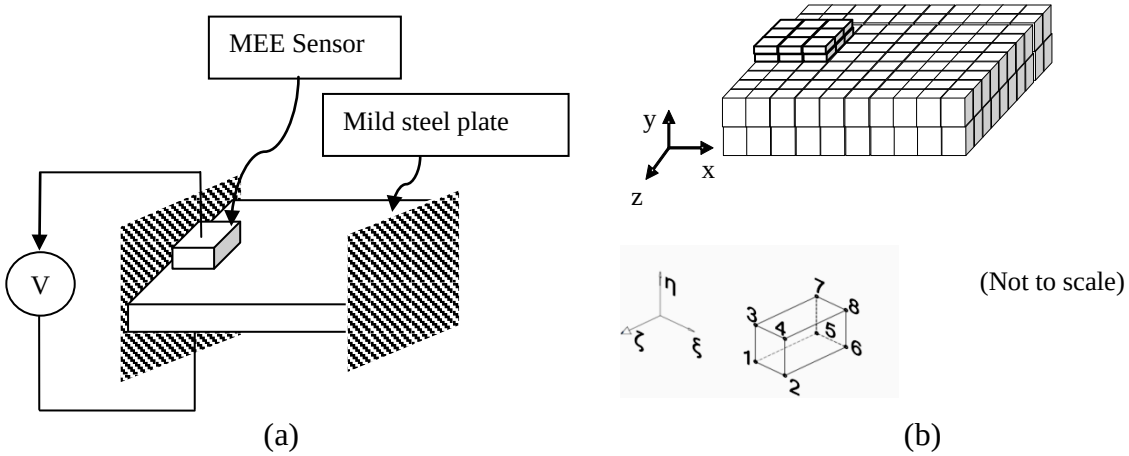

Fig. 2Schematic diagram of (a) MEE sensor bonded on mild steel plate(b) discretization with a eight-node isoparametric element.

A. Validation of the Proposed Formulation

A computer code has been developed to study the pyroeffects on the behavior of magneto-electro-elastic sensor bonded to mild steel plate subjected to various boundary conditions. The arrangement consists of one electrode from the plate which is grounded and the other electrode which is kept on the top of the sensor patch. The piezomagnetic materials can be modeled using ANSYS since the constitutive relations as well as the governing field equations (if free currents and transient effects are neglected) are of identical format with piezoelectric materials. Since ANSYS does not explicitly contain piezomagnetic relationships, it is unable to model fully coupled MEE materials which involve the combined contributions of both piezoelectric and piezomagnetic material models. Thus commercial finite element package ANSYS was used for validating the methodology adopted for solution procedure. Hence the present code is validated using piezoelectric material *PZT-5A* whose material properties (Chen *et al.*,[17]) are given in Table 1.Fig. 3shows a comparison of the longitudinal x-direction (u_x), *y*-direction (u_y) and transverse *z*-direction (u_z) displacement components and electric potential (ϕ) on the top surface of piezoelectric sensor patch along the longitudinal x-direction at the middle of the clamped edge of the sensor patch when the plate is subjected CCCC boundary condition. The results obtained by ANSYS are found to be in good agreement with the present formulation.

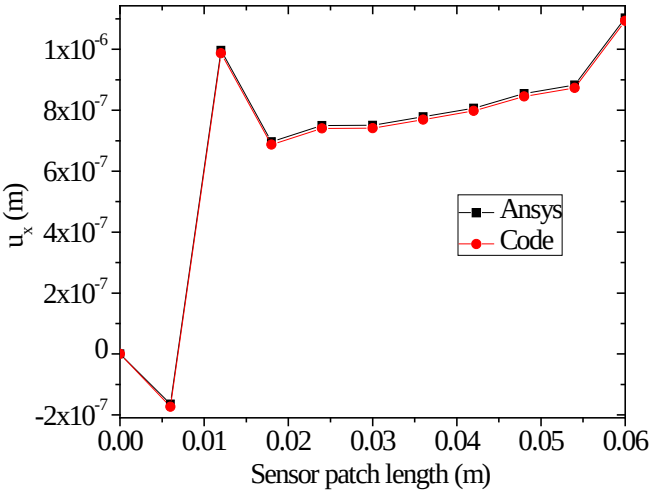
1x10-6
8x10-7
6x10-7
4x10-7
2x10-7
0
-2x10-7
ux (m)
0.00
0.01
0.02
0.03
0.04
0.05
0.06
Sensor patch length (m)
Ansys
Code

(a)

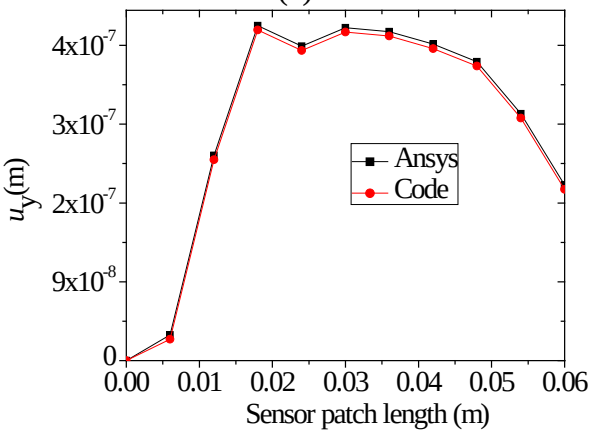
4x10-7
3x10-7
2x10-7
9x10-8
0
uy(m)
0.00
0.01
0.02
0.03
0.04
0.05
0.06
Sensor patch length (m)
Ansys
Code

(b)

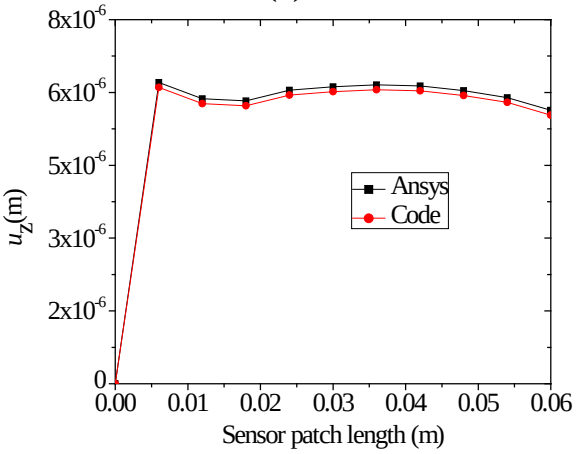
8x10-6
6x10-6
5x10-6
3x10-6
2x10-6
0
uZ(m)
0.00
0.01
0.02
0.03
0.04
0.05
0.06
Sensor patch length (m)
Ansys
Code

(c)

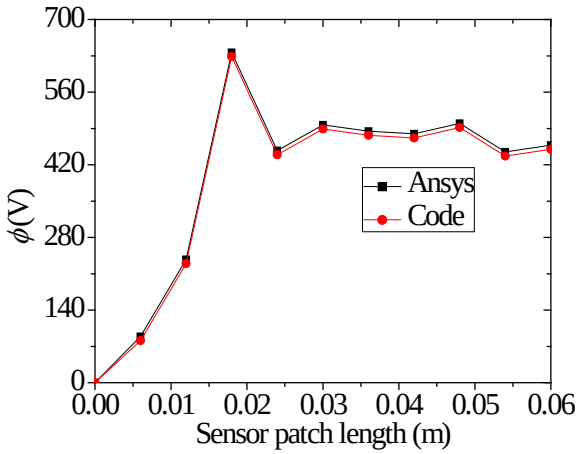

(d)

Fig. 3 Validation of (a) longitudinal x-direction (u_x), (b) y-direction (u_y), (c) transverse z-direction (u_z) displacement components and (d) electric potential (ϕ) on top surface along the longitudinal x-direction of the sensor patch (CCCC boundary condition).

B. Optimal Placement of MEE Sensor

The optimal placement of MEE sensor on top surface of the mild steel plate for maximum electric potential due to pyroelectric and pyromagnetic effects is studied. The optimal location of MEE sensor on top surface of the plate is investigated by implementing auto-mesh generation method at different positions along the length of the plate under CCCC boundary condition. The auto-mesh generation method regenerates mesh for sensor and base structure with connectivity at interface using the code incorporating the pyroelectric and pyromagnetic effects studied in this paper. It calculates the stiffness matrix and load vector at every location on the structure where the sensor is placed. It is assumed that the electric potential of the sensor is not arrested at clamped end. Fig. 4 shows the electric potential (ϕ) corresponding to the position of the MEE sensor on top surface of mild steel plate. It is observed that the electric potential is maximum near the clamped end of the plate. The pyroelectric and pyromagnetic effects on electric potential follows the same trend as that of conventional approach. This optimal location of the sensor on the plate(at the middle of the clamped edge) is considered to carry out the objective which discussed in Section III.

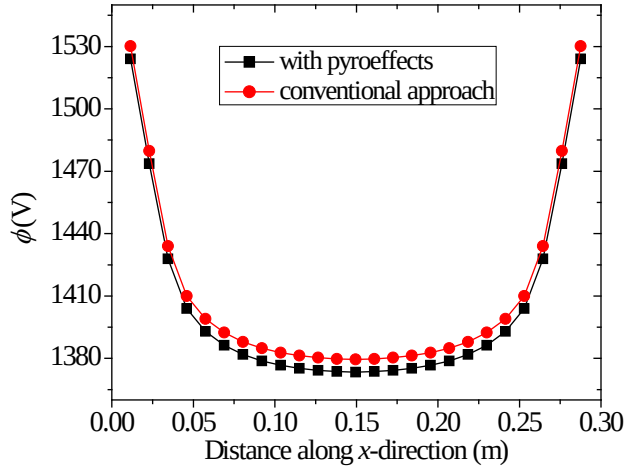

Fig. 4 Electric potential (ϕ) corresponding to the position of MEE sensor on top surface of mild steel plate under CCCC boundary conditions.

C. CCCC Boundary Condition with Sensor at Optimal Location

The sensor bonded on top surface of the plate at optimal location (at the middle of the clamped edge) is considered based on optimal sensor placement study as discussed in Section III - *B*. Fig. 5 (a)-(c) shows the longitudinal *x*-direction (u_x), *y*-direction (u_y) and transverse *z*-direction (u_z) displacement components respectively on the top surface along the longitudinal x-direction at the middle of the clamped edge of the sensor patch. It is observed that longitudinal *x*-direction and *y*-direction displacement components vary almost linearly and aremaximum at the free end of sensor patch. Transverse *z*-direction displacement component is maximum at the middle of sensor patch. Displacement components are not affected by pyroelectric and pyromagnetic effects.

Fig. 5 (d) shows variation of electric potential when sensor is placed at an optimal location. The magnitude of electric potential is maximum near the clamped end and is gradually decreasing along longitudinal *x*-direction of the plate for all volume fractions. Unlike displacement components, pyroelectric and pyromagnetic effects exists on electric potential. The variation of electric potential with pyroelectric and pyromagnetic effects follows the same trend as the conventional approach. There is a decrease in the electric potential due to pyroelectric and pyromagnetic effects. The maximum effects on electric potential is observed for the volume fraction vf = 0.2. This can be attributed to the induced strain because of the high elastic constants for vf = 0.2.

Fig. 5 (e) shows variation of magnetic potential when sensor is placed at an optimal location. There is a periodic variation in magnetic potential plot for volume fraction vf =0.0 and vf =0.2. The amplitude of the periodic variation is higher for vf =0.2. The observation is that the magnitude of magnetic potential is maximum for vf =0.2 and minimum for vf = 0.8 in the middle of the sensor patch. Unlike displacement components, pyroelectric and pyromagnetic effects depend on magnetic potential. The variation of magnetic potential with pyroelectric and pyromagnetic effects follows the same trend as the conventional approach. There is an increase in the magnetic potential due to pyroelectric and pyromagnetic effects. The maximum effects on magnetic potential is observed for the volume fraction vf = 0.2.

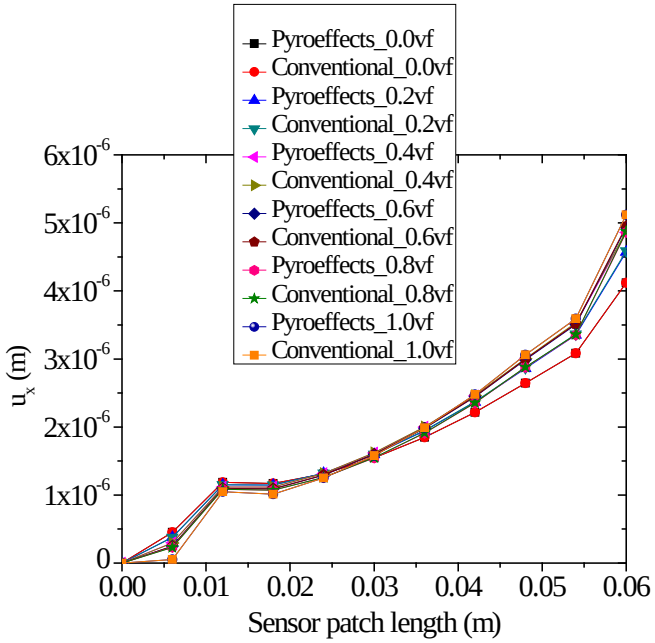

(a)

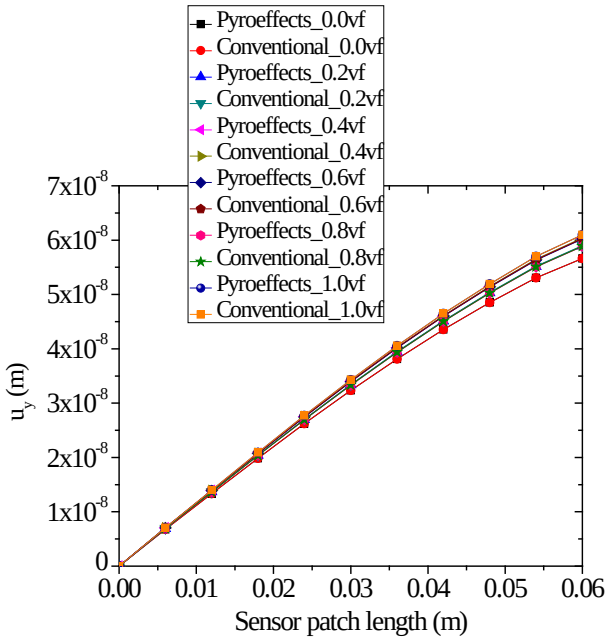
Pyroeffects_0.0vf
Conventional_0.0vf
Pyroeffects_0.2vf
Conventional_0.2vf
Pyroeffects_0.4vf
Conventional_0.4vf
Pyroeffects_0.6vf
Conventional_0.6vf
Pyroeffects_0.8vf
Conventional_0.8vf
Pyroeffects_1.0vf
Conventional_1.0vf
7x10-8
6x10-8
5x10-8
4x10-8
3x10-8
2x10-8
1x10-8
0
uy (m)
0.00
0.01
0.02
0.03
0.04
0.05
0.06
Sensor patch length (m)

(b)

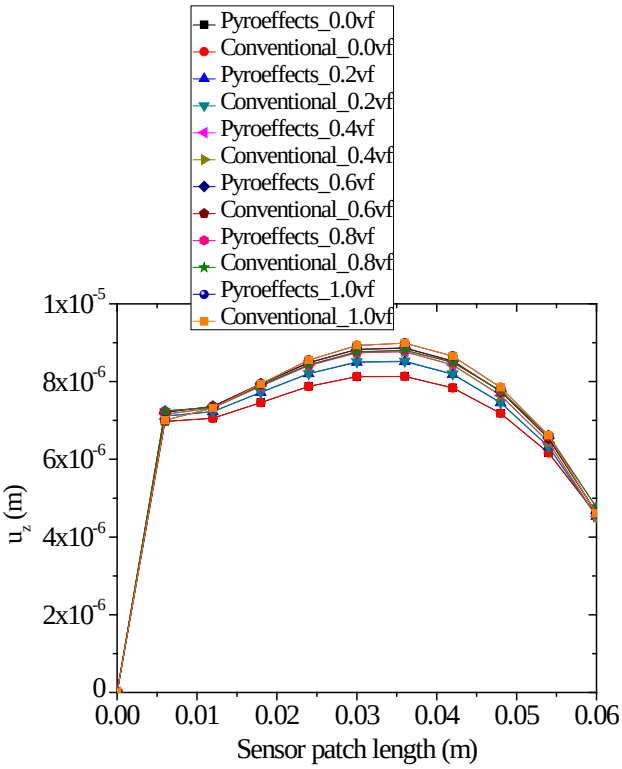
Pyroeffects_0.0vf
Conventional_0.0vf
Pyroeffects_0.2vf
Conventional_0.2vf
Pyroeffects_0.4vf
Conventional_0.4vf
Pyroeffects_0.6vf
Conventional_0.6vf
Pyroeffects_0.8vf
Conventional_0.8vf
Pyroeffects_1.0vf
Conventional_1.0vf
1x10-5
8x10-6
6x10-6
4x10-6
2x10-6
0
uz (m)
0.00
0.01
0.02
0.03
0.04
0.05
0.06
Sensor patch length (m)

(c)

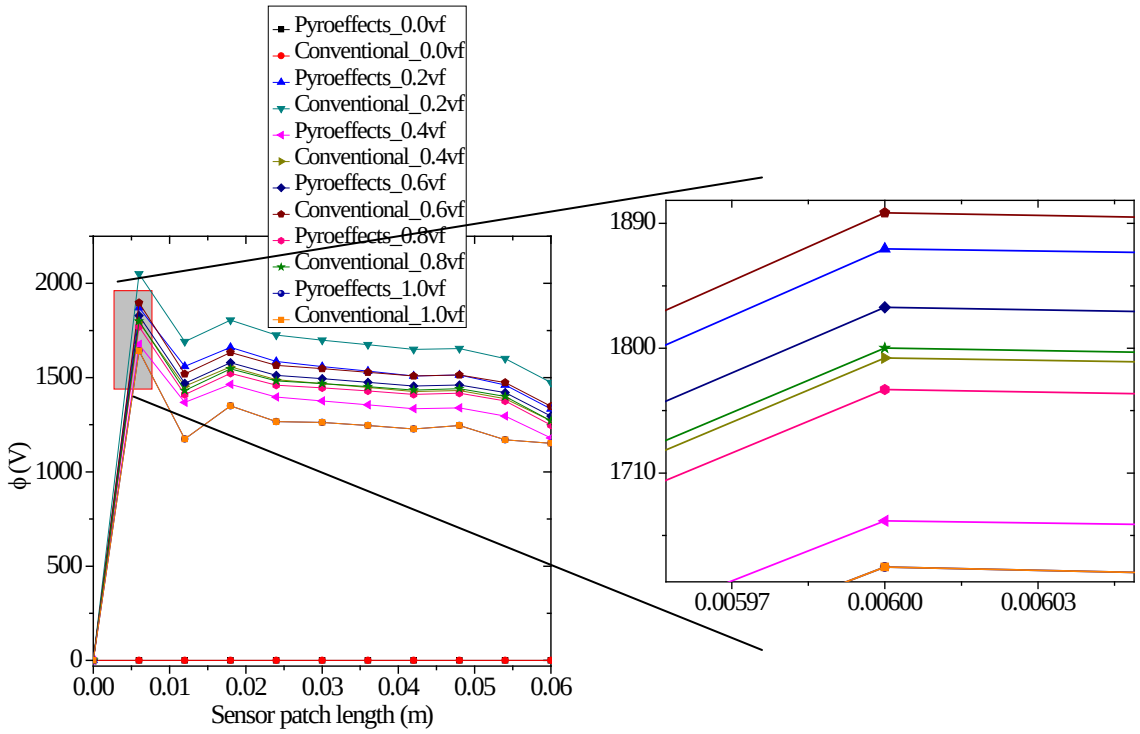

(d)

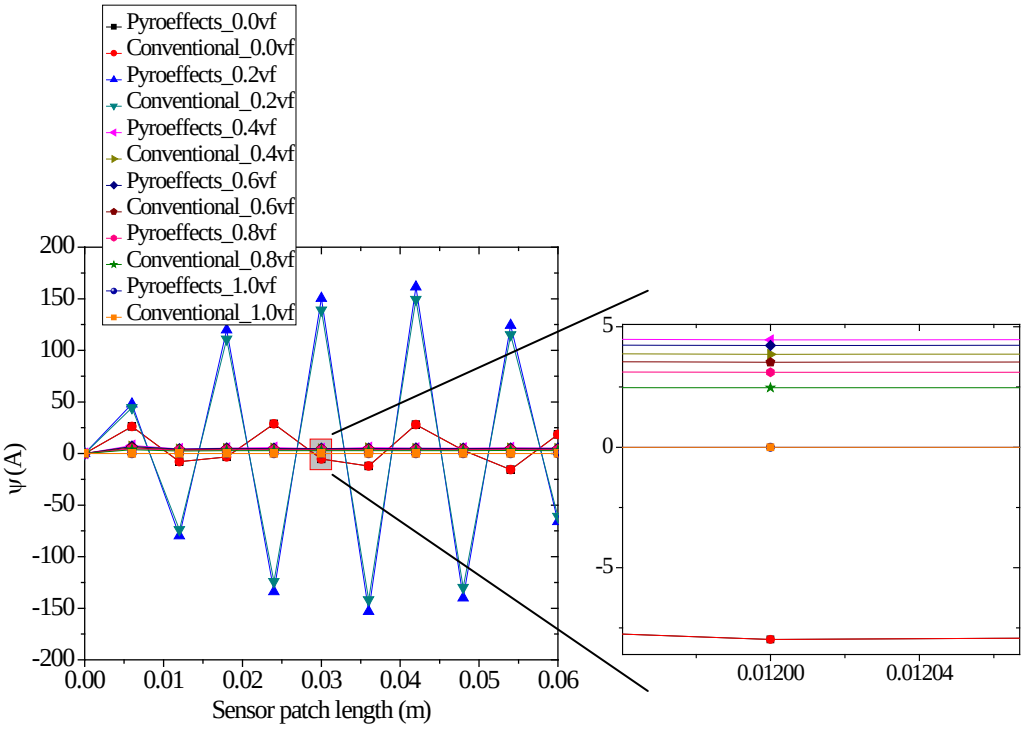

(e)

Fig. 5Variation of (a) longitudinal *x*-direction (u_x), (b) *y*-direction (u_y) and (c) transverse *z*-direction (u_z) displacement components, (d) electric (ϕ) and (e) magnetic (ψ) potentials with enlarged view on top surface along the longitudinal *x*-direction of the sensor patch (CCCC boundary condition).

D. CFFC Boundary Condition with Sensor at Optimal Location

The pyroelectric and pyromagnetic effects on the behavior of a multiphase magneto-electro-elastic sensor bonded on top surface of the plate at an optimal location (at the middle of the clamped edge) under CFFC boundary condition is studied. The study is carried out for different volume fractions of $BaTiO_3$.Similar observations are noticed for displacement components in the CFFC boundary condition as in case of previous CCCC boundary condition. Hence the displacement components are not shown.

Fig. 6(a) shows the variation of electric potential when the sensor is placed at an optimal location. The electric potential for all volume fractions give a similar outcome as in the case of CCCC boundary conditions. The magnitudes are lower in CFFC when compared to CCCC. The reason for lower magnitude maybe due to lower stress (two adjacent edges clamped) when compared to the case where all the sides are clamped. Similar observations are noticed on magnetic potential in CFFC as compared to CCCC boundary condition but with a higher magnitude.

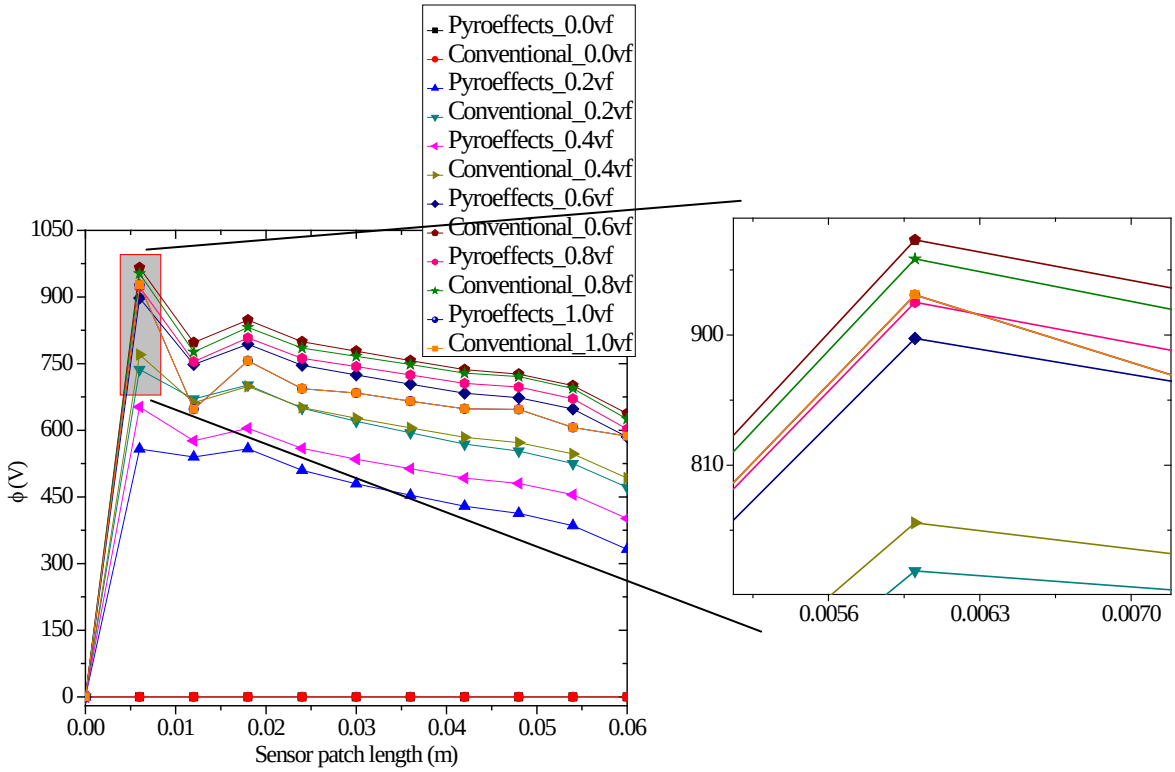

(a)

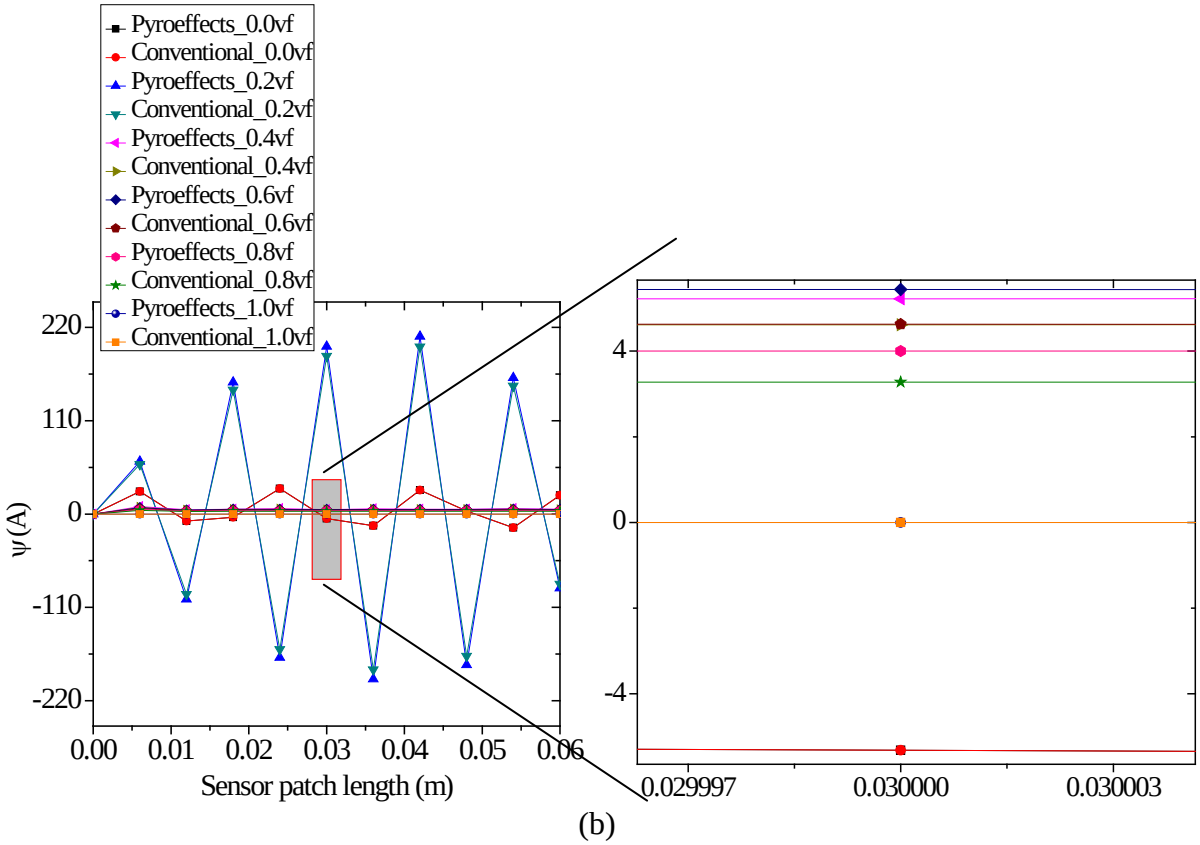

Fig 6. Variation of (a) electric (ϕ) and (b) magnetic (ψ) potentials with enlarged view on top surface along the longitudinal *x*-direction of the sensor patch (CFFC boundary condition).

E. FCFC Boundary Condition with Sensor at Optimal Location

The pyroelectric and pyromagnetic effects on behavior of multiphase magneto-electro-elastic sensor bonded on top surface of the plate at an optimal location (at the middle of the clamped edge) under CFFC boundary condition is studied. Similar observations are found on displacement components under FCFC boundary conditions as compared to CCCC and CFFC boundary conditions. Hence the displacement components are not shown.

Fig. 7(a) shows variation of electric potential when sensor is placed at an optimal location. The electric potential shows a similar observation as in CFFC. The exception being the magnitude of electric potential lies in between CFFC and CCCC. Also the magnetic potential (Fig. 7(b)) shows a similar observation as in CCCC and CFFC but the magnitude is lower than the CCCC and CFFC boundary conditions.

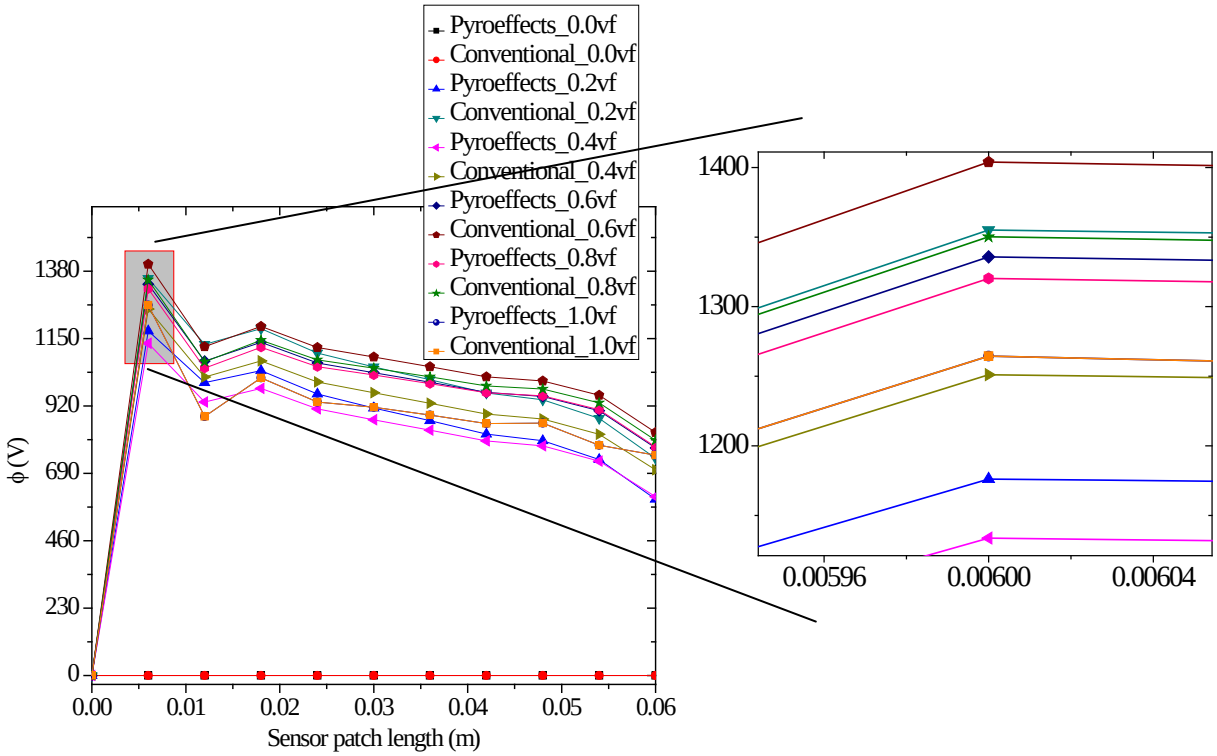

(a)

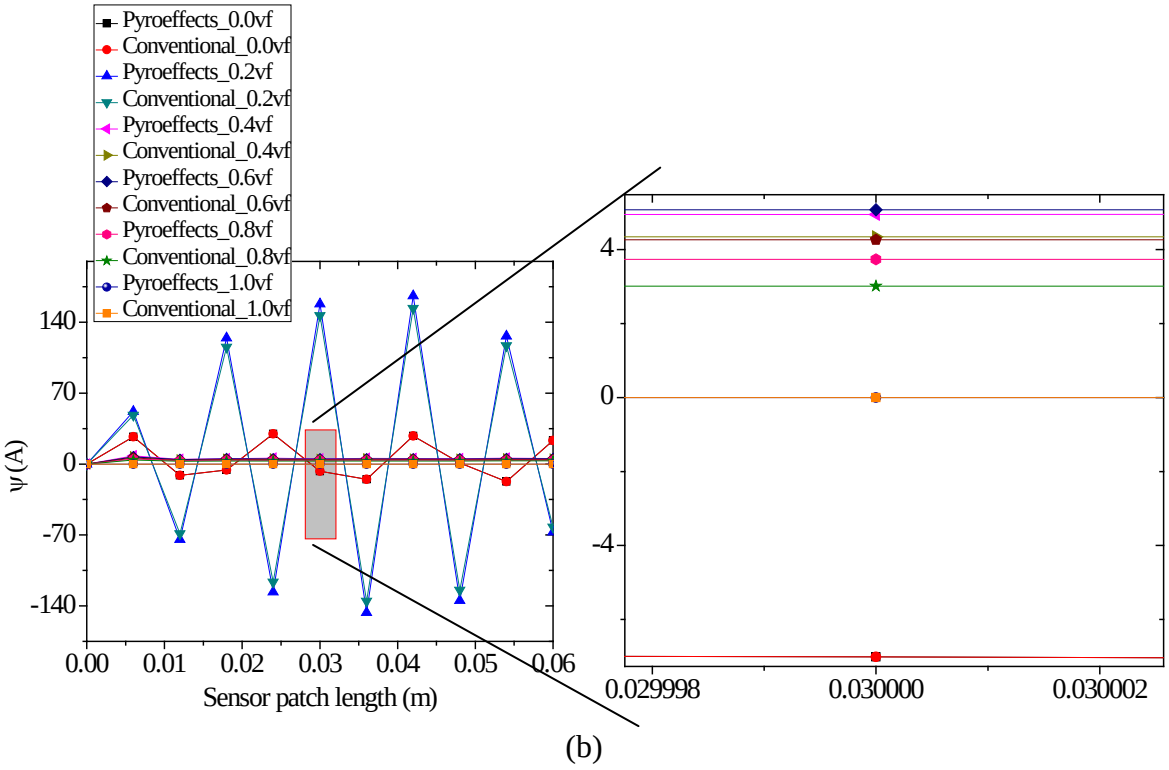

(b)

Fig 7. Variation of (a) electric (ϕ) and (b) magnetic (ψ) potentials with enlarged view on top surface along the longitudinal x-direction of the sensor patch (FCFC boundary condition).

VI. CONCLUSIONS

The pyroelectric and pyromagnetic effects on behavior of magneto-electro-elastic sensor bonded to mild steel plate under various boundary conditions (CCCC, CFFC and FCFC) is evaluated using finite element method.

- It is seen that there is no pyroelectric and pyromagnetic effects on the displacement components.
- There is an increase in magnetic potential for increasing volume fraction of the composite due to pyroelectric and pyromagnetic effects under various boundary conditions.
- The boundary conditions significantly influence the pyroelectric and pyromagnetic effects on electric and magnetic potentials for various volume fractions of the composite.
- The maximum pyroelectric and pyromagnetic effects on electric potentials is observed for volume fraction vf = 0.2 under various boundary conditions. This can be attributed to the induced strain because of the high elastic constants for vf = 0.2.

These studies will be very significant in enhancing the sensitivity of MEE sensor's electric and magnetic potentials.

REFERENCES

[1] Wu, T. L. and J. H. Huang, "Closed-form solutions for the magneto-electric coupling coefficients in Fibrous composites with piezoelectric and piezomagnetic phases", *International Journal of Solids and Structures*,37**,** pp. 2981-3009, 2000.

[2] J. Aboudi, "Micromechanical analysis of fully coupled electro-magneto-thermo-elastic multiphase composites", *Smart Mater. Structures*,vol.10, pp. 867-877, 2001.

[3] M. Sunar, A. Z. Al-Garni, M. H. Ali and R. Kahraman, "Finite element modeling of thermopiezomagnetic smart structures", *AIAA J.*,vol.40, pp.1846–51, 2002.

[4] J. Sirohi, and I. Copra, "Fundamental understanding of piezoelectric strain sensors", *J. Intell. Syst. Structures*, vol. 11, pp. 246-257, 2000.

[5] A. Mahieddine, and M. Quali, "Finite element formulation of a beam with piezoelectric patch", *J. Eng. Appl. Sci.*, vol. 3, pp. 803-807, 2008.

[6] Daga, Atul, N. Ganesan and K. Shankar, "Behavior of magneto-electro-elastic sensors under transient mechanical loading", *Sensor Actuat. A-Phys.*, vol. 150, pp. 46-55, 2009.

[7] Soh, A. K. and J. X. Liu, "On the Constitutive Equations of Magnetoelectroelastic Solids", *Journal of Intelligent Material Systems and Structures*, 16, 597-602, 2005.

[8] Ryu J., S. Priya, K. Uchino and H. E. Kim, "Magnetoelectric effect in composites of magnetostrictive and piezoelectric materials", *Journal of Electroceramics*, 8, 107–119, 2002.

[9] C. W. Nan, M. I. Bichurin, Shuxiang Dong, D. Viehland and G. Srinivasan, "Multiferroic magnetoelectric composites: Historical perspective, status, and future directions" *J. Applied Phys.*,vol.103, 031101, pp. 1-35, 2008.

[10] E. Pan and R. Wang, “Effects of geometric size and mechanical boundary conditions on magnetoelectric coupling in multiferroic composites,” *J. Phys. D: Appl. Phys.*, vol. 42, p. 7, 2009, 245503.

[11] Y. Ootao and M. Ishihara, "Exact solution of transient thermal stress problem of the multilayered magneto-electro-thermoelastic hallow cylinder", *J. Solid Mech. Mater. Engg.*, vol. 5, pp. 90-103, 2011.

[12] Guiffard B., J. W. Zhang, D. Guyomar, L. Garbuio, P. J. Cottinet, and R. Belouadah**,** "Magnetic field sensing with a single piezoelectric ceramic disk: Experiments and modeling", *Journal of Applied Physics*108, 094901, 2010.

[13] D. A. Hadjiloizi, A. V. Georgiades, Kalamkarov A L, and Jothi S, “Micromechanical Modeling of Piezo-Magneto-Thermo-Elastic Composite Structures: Part II – Theory”, *Eur. J. Mech. A. Solids*, vol. 39, pp. 313-327, 2013.

[14] J. Bravo-Castillero, R. Rodriguez-Ramos, H. Mechkour, J. Otero, and F. J. Sabina, "Homogenization of magneto-electro-elastic multilaminated materials", *Q. J. Mech. Appl. Math.*, vol. 61, pp. 311-322, 2008.

[15] C. F. Gao and N. Noda , "Thermal-induced interfacial cracking on magnetoelectroelastic materials", *International journal of engineering science*, vol. 42, pp. 1347-1360, 2004.

[16] N. Ganesan, A. Kumaravel and Raju Sethuraman, "Finite element modeling of a layered, multiphase magnetoelectroelastic cylinder subjected to an axisymmetric temperature distribution", *J. Mech. Mater. Struct.* vol. 2, pp. 655-674, 2007.

[17] J. Chen, E. Pan and H. Chen, "Wave propagation in magneto-electro-elastic multilayered plates", *Int. J. Solids Struct.*, vol. 44, pp. 1073–1085, 2007.

[18] B. Biju, N. Ganesan, and K. Shankar, "Dynamic response of multiphase magneto-electro-elastic sensors using 3D magnetic vector potential approach", *IEEE Sens. J.*, vol. 11, pp. 2169 - 2176, 2011.

[19] Melvin M Vopson, "Theory of giant-caloric effects in multiferroic materials",*J. Phys. D: Appl. Phys.*,vol. 46,345304 (7pp), 2013.

[20] Anton Fuchs, Michael J. Moser, Hubert Zangl and Thomas Bretterklieber, "Using capacitive sensing to determine the moisture content of wood pellets investigations and application", *Int. J. Smart Sensing and Intelligent Systems*,2(2), 293-308, 2009.

[21] K. B. Waghulde and Dr. Bimlesh Kumar,"Vibration Analysis of CantileverSmart Structure by usingPiezoelectricSmart Material",*Int. J. Smart Sensing and Intelligent Systems*,4(3),2011.

[22] Sauvik Banerjee, Debadatta Mandal and Shaik MahabuSubhani, "Wav let-based active sensing for health monitoring of plate structures using baseline free ultrasonic guided wave signals", *Int. J. Smart Sensing and Intelligent Systems*,6(4), 2013.

[23] B Biju, Nganesan and K Shankar,"Transient dynamic behavior of two phase magneto-electro-elastic sensors bonded to elastic rectangular plates", *Int. J. Smart Sensing and Intelligent Systems*, 5(3), 645-672, 2012.